photonics MDPI

Article

Laser Beat Wave Acceleration near Critical Density

Ernesto Barraza-Valdez [1], Toshiki Tajima[1], Donna Strickland [2] and Dante Roa [3]

[1] Department of Physics and Astronomy, University of California, Irvine; ernestob@uci.edu
[2] Department of Physics and Astronomy, University of Waterloo, Ontario, Canada;
[3] Department of Radiation Oncology, University of California, Irvine;

Abstract: We consider high density laser wakefield acceleration (LWFA) in the nonrelativistic regime of the laser. In place of an ultrashort laser pulse we can excite wakefields via the Laser Beat Wave (BW) that accesses this near-critical density regime. Here, we use 1D Particle-in-Cell (PIC) simulations to study BW acceleration using two co-propagating lasers in a near critical density material . We show that BW acceleration near the critical density allows for acceleration of electrons to greater than keV energies at far smaller intensities, such as 10^{14} W/cm^2, through the low phase velocity dynamics of wakefields that are excited in this scheme. Near-critical density laser BW acceleration has many potential applications including high dose radiation therapy.

Keywords: laser wakefield acceleration; beat wave; near critical acceleration; fiber laser; endoscopic radiotherapy;

Citation: Lastname, F.; Lastname, F.; Lastname, F. Title. *Photonics* **2022**, *9*, x. https://doi.org/10.3390/xxxxx

Received: date
Accepted: date
Published: date

1. Introduction

Laser wakefield acceleration (LWFA) allows us to make high energy acceleration of electrons [1–4]. Tajima and Dawson proposed using high intensity pulsed laser (such as 10^{18} W/cm^2) to accelerate electrons with an accelerating gradient on the order of GeV/cm [1]. Their paper launched the laser wakefield acceleration (LWFA) branch of plasma physics which was further aided by the advent of Chirped Pulse Amplifcation (CPA) and its advent also enabled LWFA realization [5]. The main allure and applications of LWFA has been to explore the energies that may not be covered easily by the conventional accelerator approaches, either in principle or by the ever-increasing cost and size of these. The energies of electrons accelerated by LWFA increase inversely proportional to the plasma density [1,3]. Thus, most of the explorations of LWFA so far have been in a density of plasma relatively far away from the critical density, the underdense regime (For a typical optical laser, the critical density is on the order of 10^{21}/cm^3), so that the typical operating plasma density has been densities of 10^{17} – 10^{19}/cm^3. This is a gaseous plasma regime.

Despite LWFA having nearly half a century of history, there has yet to be sufficient exploration of laser-plasma acceleration near the critical density. Valenta et al. determined that electron densities of roughly $0.1n_c$ were necessary for high repetition rate, low energy, short pulse lasers [6]. More recently, Nicks et al. further explored how one can achieve bulk acceleration of electrons by exploring the maximum energy achieved for different near-critical densities, laser intensities, and laser pulsewidths [4,7]. We note that in the near critical densities the gas plasma is replaced by other materials such as nanomaterials [8]. In such materials, by choosing the radius of nanotubes, for example, we can raise or reduce the average electron density that laser electromagnetic fields see. The outer shell electrons in such materials behave as if they are in a plasma state [9]. Here, we will give a brief introduction to the theory of LWFA in the underdense regime and then explore the use of laser BW near the critical density by using the well benchmarked EPOCH 1D3V (1D and 3D in spatial and velocity calculations, respectively) collisionless and relativistic Particle-in-Cell code with stationary ions [10].

This paper is structured in the following way: Section 2 will describe the theory of conventional underdense LWFA and beatwave acceleration (BWA). Section 3 will describe BWA at near critical densities and show results of PIC simulations with low intensity lasers and near critical density plasma targets. Section 4 will discuss applications to medicine. Section 5 will summarize and conclude this paper.

2. Underdense LWFA and BWA

LWFA in underdense plasma operates where the plasma density is much lower than the critical density $n_e \ll n_c$. Through the Stimulated Raman Scattering (SRS) process [11,12], an electromagnetic wave excites a plasma wave with ω_p following the frequency or energy conservation of:

$$\omega_p = \omega_0 - \omega_1 \,, \tag{1}$$

where $\omega_p = \sqrt{4\pi n_e e^2/m}$ and the 'p' subscript denotes electron plasma, n_e is the electron plasma density, 'e' is the electron charge, and m is the electron mass. Following the above frequency equation where ω_0 is the incident wave and ω_1 is the scattered wave, whilst also conserving wave number (or momentum) such that $\boldsymbol{k_p} = \boldsymbol{k_0} - \boldsymbol{k_1}$.

Similarly, Rosenbluth and Liu derived the process of exciting plasma waves using the beat wave of two lasers such that frequency difference was equal to the plasma frequency following Equation 1 [13,14]. This is beat wave (BW) excitation of plasma waves. When the two lasers are co-propagating, the Forward Raman Scattering (FRS) mechanism becomes significant and electrons can then be accelerated by the plasma waves [2,11,14–16]. We classify this as Beatwave Acceleration (BWA). If laser fields for the pump $\boldsymbol{E_0}$ (higher frequency) and seed $\boldsymbol{E_1}$ (lower frequency) are near the relativistic range of $\propto m\omega_0 c/e$ then the ponderomotive force created by the beatwave of the two lasers drives an electrostatic longitudinal plasma wave $\boldsymbol{E_L}$ such that:

$$eE_L \;=\; \nabla\left(\frac{e\boldsymbol{E_0}\cdot\boldsymbol{E_1}}{m\omega_0\omega_1}\right) = \; e\left(\frac{m\omega_p c}{e}\right)e^{i\,k_p x}. \tag{2}$$

The phase velocity of this electrostatic wave (plasmon) is thus:

$$v_{ph} = \frac{\omega_p}{k_p} = \frac{\omega_0 - \omega_1}{k_0 - k_1}\,. \tag{3}$$

In the limit of highly underdense plasma $\omega_p/\omega_0 \ll 1$: $v_{ph} = \frac{\omega_p}{k_p} \approx c$. Here we use the dispersion relation for an electromagnetic wave (photon) in a highly under dense plasma [17]:

$$\omega = ck/\sqrt{1 - \omega_p^2/\omega^2}\,. \tag{4}$$

With this one can see that the phase velocity of the plasmon wave matches the group velocity of a photon when $\omega_0, \omega_1 \gg \omega_p$:

$$v_g = \frac{\partial\omega}{\partial k} = \frac{c}{\omega}\sqrt{1 - n_e/n_c}\,, \tag{5}$$

where n_c is the critical density of a laser. In the rest of this paper, n_c refers to the critical density of the lowest frequency wave (seed).

Therefore, in a highly underdense plasma the laser frequency $\omega \gg \omega_p$ and both the laser phase velocity and group velocity reduce to $v_{ph} \;\approx\; v_g \;\approx\; c$. This is shown in Figure 1, where the 2D Fast Fourier Transform (FFT) of the transverse and longitudinal electric field of the laser beatwave PIC simulation in an underdense plasma ($n_e = 0.005 \times n_c$) is plotted and shows the dispersion.

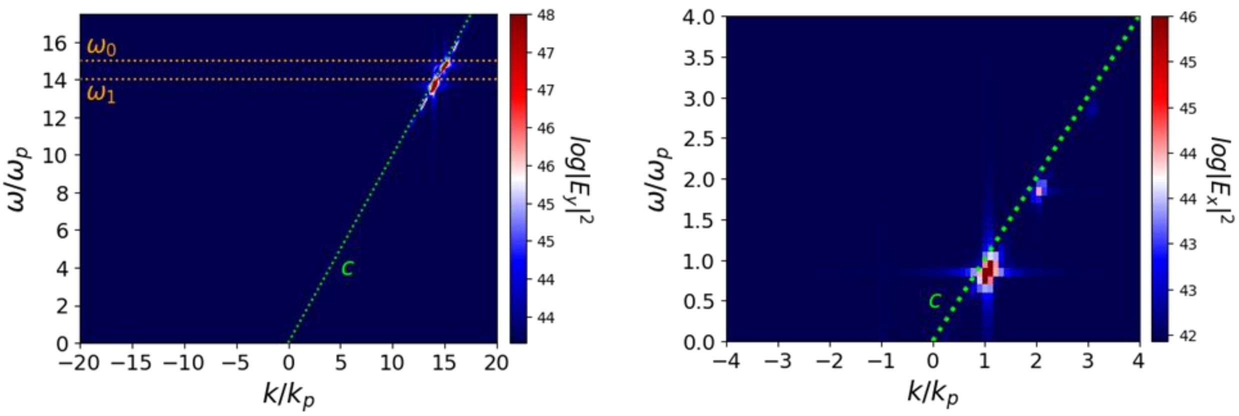

(**a**) (**b**)

Figure 1. The 2D Fast Fourier Transform (FFT) of the (**a**) transverse (E_y) and (**b**) longitudinal (E_x) electric field in a 1D PIC simulation of highly underdense laser BW acceleration normalized to the normalized to the plasma frequency (ω_p) and plasma wave number ($k_p = \omega_p/c$). ω_0 and ω_1 are the two copropagating laser frequencies of the beatwave, indicated by the orange dotted lines in (**a**). The diverging color indicates the intensity of the fields in logscale. The speed of light dispersion (slope) is indicated by the lime green dotted line.

The laser beatwave excites longitudinal electrostatic wakefields with a phase velocity near c in low density plasma. A high phase velocity, much larger than the thermal velocity, allows the plasma wave to be stable and coherent against thermal plasma instabilities and allows the lasers to drive the plasma wave until saturation. Conventionally, the strength of the plasmons derives from the ponderomotive force described by Tajima and Dawson, which gives us a maximum electrostatic field of [14]:

$$E_{L,max} = E_{wb} = \frac{m\omega_p c}{e}, \tag{6}$$

which is the well known electrostatic wavebreaking field in the cold plasma approximation.

With the wake waves' high phase velocity, far away from the bulk thermal velocity of the plasma, the strength of these wakes will have to grow large enough to be able to trap electrons from the fringes of the thermal distribution and accelerate them. If the amplitude of the wake waves are not strong enough, electrons will need to be externally injected at the high enough energies in order to be trapped. The range of velocities (energies) that the excited wake waves can trap and accelerate electrons is described by the trapping width velocity [18]:

$$v_{trap} = \sqrt{eE_L/mk}, \tag{7}$$

where E_L is the amplitude of the wake wave and k is its wave number. Thus, because $v_{ph} \gg v_{th}$ the wave number k is small, making the trapping width small. Wakes cannot functionally trap and accelerate electrons from the bulk plasma thermal distribution. This again reinforces that the laser and wakes are stable from thermal plasma instabilities. Figure 2 shows the electric field and phase space of this highly underdense BW simulation. One can see that only at relativistic laser intensities ($a_0 \geq 1$) is the electrostatic wake amplitude driven large enough to trap a small population of electrons from the tail end of the thermal distribution and accelerate them.

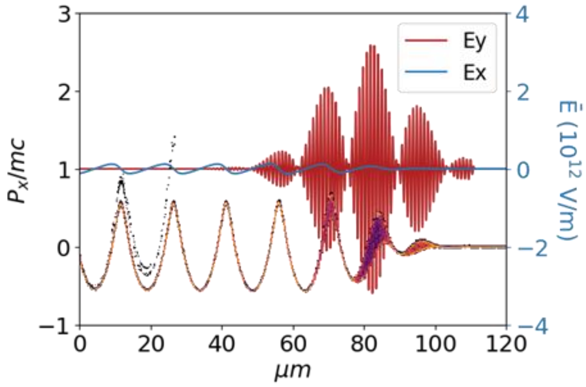

Figure 2. Electron phase space plot with electric fields of a 1D PIC simulation at 150 fs. The momentum is normalized to electron mass times the speed of light (c) on the left most y-scale vs the position in the horizontal axis. The sequential color scale indicates the population density of electrons in that particular phase space point where bright orange indicates a large amount and purple or dark colors indicate small populations. The electric fields are indicated by the transverse y- (red) and longitudinal x- (blue) lines representing the laser and plasmon fields respectively. This simulation used an equivalent of $a_0 = 1$, beatwave laser wavelengths of 0.5 μm and 1 μm with 100 fs pulswidth and $n_e = 0.005 \times n_c$.

In the relativistic regime, the saturation due to relativistic mass and detuning effects gives the saturated electrostatic field to be [2,13]:

$$E_L = \frac{m\omega_p c}{e}\left(\frac{16}{3}a_0 a_1\right)^{\frac{1}{3}}, \tag{8}$$

where $a_{0,1} = \frac{e|\boldsymbol{E}_{0,1}|}{m\omega_{0,1}c}$ is the normalized laser vector potentials for the pump, indicated by the 0 subscript, and the seed, the 1 subscript. The maximum acceleration energy of trapped electrons is:

$$W_{max} = 2\,a_0\,\gamma^2 mc^2 \;\propto\; a_0^2\left(\frac{\omega_0}{\omega_p}\right)^2, \tag{9}$$

where γ is the Lorentz factor. For non-relativistic (nr), low intensities ($a_0 < 1$), in an underdense plasma ($n_c >> n_e$) we have no factor $2\gamma^2$ (due to the relativistic dynamics of the phase velocity of the wake for the relativistically extended dephasing length). If we assume in this case that the dephasing length is simply $\frac{\pi\, c}{2\,\omega_p}$ we obtain the low intensity maximum electron energy, while the ponderomotive force in the nonrelativistic regime is proportional to a_0^2, which may lead to an expression such as $W_{max,nr} = \frac{\pi}{2}mv_{ph}^2 a_0^2\left(\frac{\omega_0}{\omega_p}\right)$. This type of energy would apply if the wakefield with nonrelativistic amplitude is excited but remains as a single wave. As we will see below, however, in the high density regime of wakefields (near the critical density), we observe that a series of wakefields with different phase velocities tend to be excited.

Nicks et al showed electron energy scaling with respect to laser intensity ($1 > a_0 \geq 0.1$) for $0.1n_e$ and $0.3n_e$ in Figure 5a,b [7]. Nicks et al showed that a somewhat discontinuous maximum energy gain of electrons as a function of a_0 (around 1) is observed. This arises from the transition between the nonrelativistic wakefields dynamics ($a_0 < 1$) and the relativistic one ($a_0 \geq 1$) .

3. Near Critical Density BWA

When n_e is near the critical density, additional physics comes into play. With lower laser intensities, low phase velocity (which means a density very close to the critical density) or external electron injection mechanisms are needed to allow for electrons to interact with the wakefields and be accelerated. We show that near critical densities allow for the excitation of low phase velocity plasmons and introduces the opportunity to pick up electrons in the bulk which would not be possible in the conventional underdense operation of LWFA. This high density, low intensity LWFA scheme makes it suitable for many applications.

For many industrial and medical applications, electron energies of greater than keV are required with low laser intensities of ≤ 10^{14} W/cm^2 (corresponding to $a_0 < 0.01$ for a 1 μm laser). For a 1 μm laser, the critical density is approximately 10^{21} cm^3 which is about one order of magnitude less than a conventional solid. This high density allows the BW accelerator to be done in ambient pressure rather than vacuum. Thus, our study will focus on using a 1 μm laser with plasma densities of approximately $n_e \approx 0.9 \times n_c \approx 0.9 \cdot 10^{21}$ cm^{-3}.

The excitation of low phase velocity plasmons with much lower laser intensities lends itself to the Enhanced Raman Forward Scattering (ERFS) method [19]. In the ERFS method, the laser intensities need not be equal as in the conventional BW case. Fisher and Tajima showed that ERFS allows for the lower frequency seed (ω_1) laser's intensity to be 10% of the higher frequency pump (ω_0) laser's intensity. In this case, the lower frequency laser seeds the growth of the plasma wave but there are also other seeding methods such as pulse shaping and electrostatic plasmon seeding. The smaller seed intensity further allows the usage of modern table top laser technology.

We now turn to the exploration of low intensity, non-relativistic BW acceleration using the EFRS method. To represent a thin target of density 0.9×10^{21} cm^3 in the simulation, the plasma is set to be between 1-20 μm thick (with ions left to be infinitely heavier and stationary). Figure 3 shows the transverse and longitudinal field spectrum for 20 μm thick plasma. Figure 3a is similar to Figure 1a except that the seed frequency is now just above the plasma frequency ($\omega_1 \approx 1.1\ \omega_p$). Additionally, the lasers propagate freely in vacuum before hitting the target. The free space propagation is clearly shown by the spectrum points that align with the speed of light in vacuum (lime green). In Figure 3b, one can see that there is excitation at ω_p with a broad range of wavenumber. This is due to nonlinear parametric processes and is allowed by the high density plasma (near critical) so that their phase velocities are low. The allowed group velocity of the photons is small and so the ponderomotive force can push electrons whose velocities may come in resonance with multiple of small phase velocity plasma waves. This allowed wide range of the phase velocities in nonrelativitic wakefields is the reason why we see this wide spectrum of plasma waves.

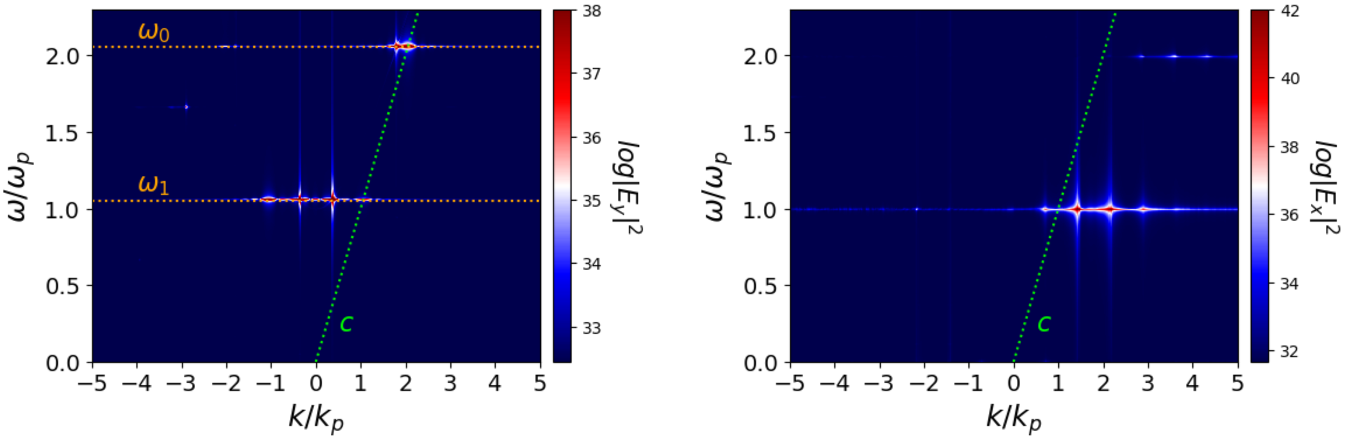

(**a**) (**b**)

Figure 3. 2D Fast Fourier Transform (FFT) of the (a) transverse (E_y) and (b) longitudinal (E_x) electric field in a 1D PIC simulation of BW acceleration near the critical density

Figure 4 shows the phase space and electric field components for this simulation using a laser intensity of 2.5 x 10[14] W/cm[2] (a_0 = 0.007) with a pulse width of 2 ps. One can see that at 2 ps, the tail end of the laser pulses, the longitudinal plasma wave amplitude has grown larger than the pump laser's amplitude. At 2.5 ps, the laser has left the simulation and one can see the strong plasma waves continue unimpeded and are able to accelerate electrons to keV energies.

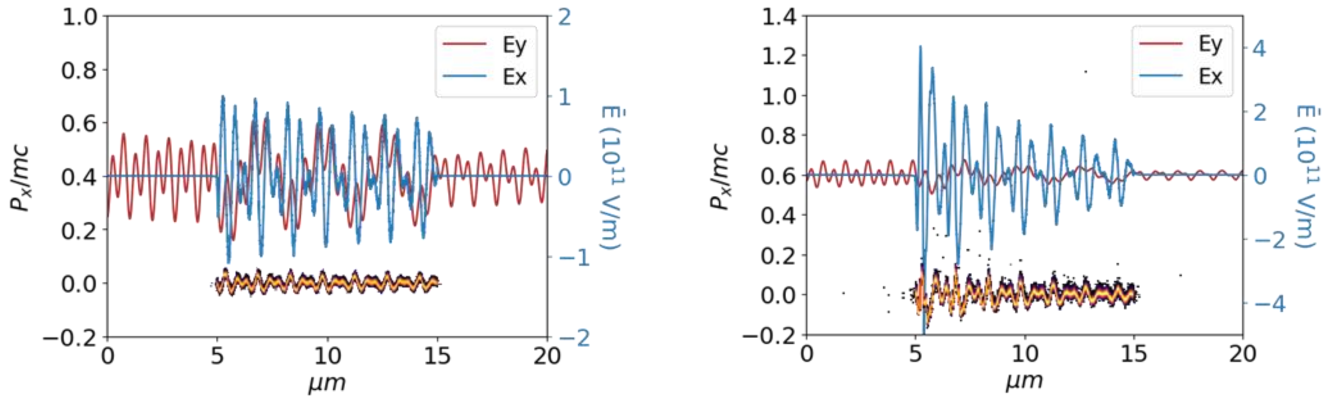

(**a**) (**b**)

Figure 4. This is a figure Phase space distribution and transverse and longitudinal electric fields for a 1D 10 μm plasma target at (a) 2 ps and (b) 2.5 ps. The EFRS method is used with a_0 = 0.007 (2.5 x 10[14] W/cm[2]) and a_1 = 0.004 (9.7 x 10[13] W/cm[2]) and n_e = $0.9 \times n_c$, $\lambda_0 \approx 0.5$ μm and $\lambda_1 = 1.0$ μm, and the pulsewidth is 2 ps.

Figure 5 shows the electron energies with respect to different simulations. Figure 5a shows the electron energy distribution after 2.5 ps for varying thicknesses of the plasma-target. One can see that that below 5 μm, electrons are just barely accelerated above keV energies. This is most likely because the main plasma wave in the mix of wakefields is the one with a phase velocity near c so that the main plasma wavelength corresponds to approximately 1 μm, this is confirmed by Figure 4. Thus, for small thicknesses there is not enough wake waves to accelerate electrons. However, there does not seem to be more enhancement in the electron energy spectrum as the plasma thickness is increased.

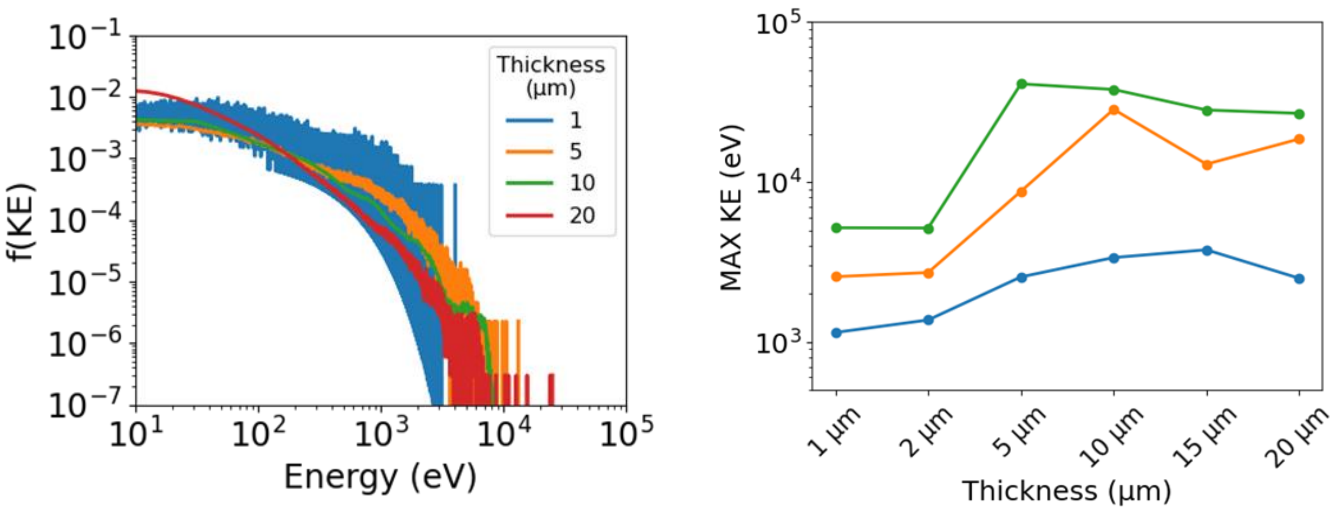

(**a**) (**b**)

Figure 5. (a) The energy distribution of thin plasma target simulation after 2.5 ps with change of thickness. The intensity of the pump wave 2.5 x 10[14] W/cm[-2] and the seed intensity was one-tenth of that ($a_0 = \sqrt{10} \cdot a_1$). Pulsewidth of 2 ps. (b) Maximum kinetic energy

(y-axis) of an electron found in simulation after 2.5 ps with respect to thickness (x-axis) given different laser parameters: (blue) 1.3 x 10[14] W/cm[-2] pump ($a_0 = 0.005$) with a pulsewidth of 2 ps, (yellow) 2.5 x 10[14] W/cm[-2] pump ($a_0 = 0.007$) with a pulsewidth of 1 ps, (green) 2.5 x 10[14] W/cm[-2] pump ($a_0 = 0.007$) with a pulsewidth of 2 ps.

In order to make this acceleration scheme more applicable, lower laser intensities than 2.5 x 10^{14} W/cm^2 are chosen. Figure 5b shows the maximum kinetic energy found in the simulation after 2.5 ps for three different laser parameters: 1.3 x 10^{14} W/cm^2 with 2 ps pulsewidth, and 2.5 x 10^{14} W/cm^2 with 1 ps and 2 ps pulsewidth. One can see that the intensity allows for higher electron energies, which is expected. In addition, increasing the pulswidth to deliver more energy also increases the maximum kinetic energy that the electrons can achieve. Below 1.3 x 10^{14} W/cm^2 ($a_0 < 0.005$), we saw that the plasma waves continued to grow beyond 2.5ps.

4. Applications to Medicine

As we have found, the high density operation (near the critical density) LWFA opens an avenue to make very compact electron acceleration (though electron energies are modest such as 10's keV) with modest laser intensity. The near-critical density exceeds the usual gaseous plasma density. The opportunity of using carbon nanotubes (and possibly other nanomaterials) to match this regime of density with changing its occupation ratio (such as the tube diameter) introduces an added flexibility and value of this regime operation [8,20]. We no longer need the vacuum to hold gas plasma. Also, this brings in a flexible density ramping, if desired or necessary, for additional control in the acceleration process. The size of the target in this high density LWFA further reduces the size of the accelerator from even the gaseous LWFA, which is already far smaller than the conventional accelerators.

Additionally, near critical density LWFA lends itself to low intensity schemes such as EFRS. This allows the seed laser intensity to be 10% of the pump laser's and still achieve 10's keV electron energies.

Meanwhile, if and when we can use an electron accelerator so tiny that it can sit in front of the tumor of a patient (such as at the tip of an endoscope), the electrons for radiotherapy purpose need not to have MeV of energies, as they do not have to penetrate patient's body. In this case, the needed electron energies may be as low as 10's keV. The penetration depth of such electrons is short and reaches only the tissues that is facing the accelerator at the tip of the device such as an endoscope. This study shows that our present regime of laser intensity and operation are within the reach of the fiber laser technology, see [21]. Accordingly, this introduces a new possible way to operate an endoscopic electron radiotherapy using fiber laser. That is, an endoscopic radiation therapy. The surgeon would enter internal part of a patient with an endoscope that has attached the HD LWFA at its tip. When he/she sees a tumor, he/she can turn on the HD LWFA at its suspected tumor. It could also be used to spray electrons after the surgical removal of a macroscopic tumor by endoscope, to make sure the remaining tissue can be devoid of active tumors (it may also be delivered as part of an acupuncture needle).

Such electrons may be used to address other therapy such as allowing for handheld radiation therapy device that can directly target superficial skin cancers such as melanoma [22–25]. Further, we could also employ a vector medicine (with high Z) that can guide itself toward the targeted tissue (such as cancer cells) that attracts and absorbs preferentially electrons to the vector molecules with its high Z distinction [26].

5. Conclusions

To summarize, we used the well benchmarked 1D3V relativistic PIC code EPOCH and showed the dynamics of LWFA and BWA in underdense plasmas and near critical density plasmas. In Section 2, conventional LWFA was discussed. Conventional LWFA relies on an high laser intensities and underdense plasmas so that the group velocity of the laser ($\approx c$) can excite longitudinal plasma waves with similar phase velocity. Thus, a robust and coherent plasma wave train is excited with immunity from thermal plasma instabilities. It is conventional wisdom that lower plasma density allows for more stable wake waves and therefore larger electron energy accelerations as shown in Equation 9 [4].

In Section 3, we studied a low intensity EFRS scheme to accelerate electrons to keV energies using low intensity lasers (approximately 10^{15} W/cm^2) near the critical density. At the near critical densities, we have shown that using laser BW with the ERFS method, nonlinear processes are excited. One of these processes is the growth of a multiple small phase velocity plasma waves rather than the single large phase velocity wakefield, shown in Figure 3. This ensemble of plasmon waves with low phase velocities allows for efficient trapping of electrons from the bulk thermal distribution.

The EFRS scheme in a thin target has two advantages: the use of low intensity lasers and microscopic acceleration length. The microscopic acceleration length is beneficial in many industrial and medical applications as discussed in Section 4.

Author Contributions: Conceptualization, Toshiki Tajima; Data curation, Ernesto Barraza-Valdez; Formal analysis, Ernesto Barraza-Valdez; Funding acquisition, Toshiki Tajima; Investigation, Ernesto Barraza-Valdez; Methodology, Ernesto Barraza-Valdez; Software, Ernesto Barraza-Valdez; Supervision, Toshiki Tajima; Validation, Ernesto Barraza-Valdez; Visualization, Ernesto Barraza-Valdez; Writing – original draft, Ernesto Barraza-Valdez and Toshiki Tajima; Writing – review & editing, Toshiki Tajima, Donna Strickland and Dante Roa.

Funding: The work was in part supported by the Rostoker Fund.

Acknowledgments: We benefitted a great deal of advices and inspirations specifically on this or in general over the years from Dr. W. J. Sha, Dr. J. C. Chanteloup, Prof. G. Mourou, Prof. S. Iijima, and Prof. F. Tamanoi. For these we are very grateful.

References

1. Tajima, T.; Dawson, J.M. Laser Electron Accelerator. *Phys. Rev. Lett.* **1979**, *43*, 267–270, doi:10.1103/PhysRevLett.43.267.
2. Tajima, T. High Energy Laser Plasma Accelerators. *Laser and Particle Beams* **1985**, *3*, 351–413, doi:10.1017/S0263034600001117.
3. Esarey, E.; Schroeder, C.B.; Leemans, W.P. Physics of Laser-Driven Plasma-Based Electron Accelerators. *Rev. Mod. Phys.* **2009**, *81*, 1229–1285, doi:10.1103/RevModPhys.81.1229.
4. Tajima, T.; Yan, X.Q.; Ebisuzaki, T. Wakefield Acceleration. *Rev. Mod. Plasma Phys.* **2020**, *4*, 7, doi:10.1007/s41614-020-0043-z.
5. Strickland, D.; Mourou, G. Compression of Amplified Chirped Optical Pulses. *Optics Communications* **1985**, *55*, 447–449, doi:10.1016/0030-4018(85)90151-8.
6. Valenta, P.; Klimo, O.; Grittani, G.M.; Esirkepov, T.Z.; Korn, G.; Bulanov, S.V. Wakefield Excited by Ultrashort Laser Pulses in Near-Critical Density Plasmas. In Proceedings of the Laser Acceleration of Electrons, Protons, and Ions V; SPIE, April 24 2019; Vol. 11037, pp. 57–65.
7. Nicks, B.S.; Barraza-Valdez, E.; Hakimi, S.; Chesnut, K.; DeGrandchamp, G.; Gage, K.; Housley, D.; Huxtable, G.; Lawler, G.; Lin, D.; et al. High-Density Dynamics of Laser Wakefield Acceleration from Gas Plasmas to Nanotubes. *Photonics* **2021**, *8*, 216, doi:10.3390/photonics8060216.
8. Iijima, S. Helical Microtubules of Graphitic Carbon. *Nature* **1991**, *354*, 56–58, doi:10.1038/354056a0.
9. Zhang, X.; Tajima, T.; Farinella, D.; Shin, Y.; Mourou, G.; Wheeler, J.; Taborek, P.; Chen, P.; Dollar, F.; Shen, B. Particle-in-Cell Simulation of x-Ray Wakefield Acceleration and Betatron Radiation in Nanotubes. *Phys. Rev. Accel. Beams* **2016**, *19*, 101004, doi:10.1103/PhysRevAccelBeams.19.101004.

10. Arber, T.D.; Bennett, K.; Brady, C.S.; Lawrence-Douglas, A.; Ramsay, M.G.; Sircombe, N.J.; Gillies, P.; Evans, R.G.; Schmitz, H.; Bell, A.R.; et al. Contemporary Particle-in-Cell Approach to Laser-Plasma Modelling. *Plasma Phys. Control. Fusion* **2015**, *57*, 113001, doi:10.1088/0741-3335/57/11/113001.
11. Shen, Y.R.; Bloembergen, N. Theory of Stimulated Brillouin and Raman Scattering. *Phys. Rev.* **1965**, *137*, A1787–A1805, doi:10.1103/PhysRev.137.A1787.
12. Liu, C.S.; Rosenbluth, M.N.; White, R.B. Raman and Brillouin Scattering of Electromagnetic Waves in Inhomogeneous Plasmas. *The Physics of Fluids* **1974**, *17*, 1211–1219, doi:10.1063/1.1694867.
13. Rosenbluth, M.N.; Liu, C.S. Excitation of Plasma Waves by Two Laser Beams. *Phys. Rev. Lett.* **1972**, *29*, 701–705, doi:10.1103/PhysRevLett.29.701.
14. Tajima, T.; Dawson, J.M. Laser Beat Accelerator. *IEEE Transactions on Nuclear Science* **1981**, *28*, 3416–3417, doi:10.1109/TNS.1981.4332122.
15. Joshi, C.; Tajima, T.; Dawson, J.M.; Baldis, H.A.; Ebrahim, N.A. Forward Raman Instability and Electron Acceleration. *Phys. Rev. Lett.* **1981**, *47*, 1285–1288, doi:10.1103/PhysRevLett.47.1285.
16. Horton, W.; Tajima, T. Laser Beat-Wave Accelerator and Plasma Noise. *Phys. Rev. A* **1985**, *31*, 3937–3946, doi:10.1103/PhysRevA.31.3937.
17. Ginzburg, V.L. *The Propagation of Electromagnetic Waves in Plasmas*; International series of monographs on electromagnetic waves, v. 7; 2d ed., rev.enl.; Pergamon Press: Oxford, New York, 1970; ISBN 978-0-08-015569-2.
18. O'Neil, T. Collisionless Damping of Nonlinear Plasma Oscillations. *The Physics of Fluids* **1965**, *8*, 2255–2262, doi:10.1063/1.1761193.
19. Fisher, D.L.; Tajima, T. Enhanced Raman Forward Scattering. *Phys. Rev. E* **1996**, *53*, 1844–1851, doi:10.1103/PhysRevE.53.1844.
20. *Beam Acceleration in Crystals and Nanostructures*; Chattopadhyay, S., Mourou, G., Shiltsev, V.D., Tajima, T., Eds.; World Scientific: New Jersey London Singapore Beijing Shanghai Hong Kong Taipei Chennai Tokyo, 2020; ISBN 9789811217135.
21. Sha, W.J.; Chanteloup, J.C.; Mourou, G. *Photonics (forthcoming)*.
22. Nicks, B.S.; Tajima, T.; Roa, D.; Ne?as, A.; Mourou, G. Laser-Wakefield Application to Oncology. In *Beam Acceleration in Crystals and Nanostructures*; WORLD SCIENTIFIC, 2020; pp. 223–236 ISBN 9789811217128.
23. Roa, D.; Leon, S.; Paucar, O.; Gonzales, A.; Schwarz, B.; Olguin, E.; Moskvin, V.; Alva-Sanchez, M.; Glassell, M.; Correa, N.; et al. Monte Carlo Simulations and Phantom Validation of Low-Dose Radiotherapy to the Lungs Using an Interventional Radiology C-Arm Fluoroscope. *Physica Medica* **2022**, *94*, 24–34, doi:10.1016/j.ejmp.2021.12.014.
24. Veness, M.; Richards, S. Role of Modern Radiotherapy in Treating Skin Cancer. *Australasian Journal of Dermatology* **2003**, *44*, 159–168, doi:10.1046/j.1440-0960.2003.06711.x.
25. Mierzwa, M.L. Radiotherapy for Skin Cancers of the Face, Head, and Neck. *Facial Plastic Surgery Clinics* **2019**, *27*, 131–138, doi:10.1016/j.fsc.2018.08.005.
26. Matsumoto, K.; Saitoh, H.; Doan, T.L.H.; Shiro, A.; Nakai, K.; Komatsu, A.; Tsujimoto, M.; Yasuda, R.; Kawachi, T.; Tajima, T.; et al. Destruction of Tumor Mass by Gadolinium-Loaded Nanoparticles Irradiated with Monochromatic X-Rays: Implications for the Auger Therapy. *Sci Rep* **2019**, *9*, 13275, doi:10.1038/s41598-019-49978-1.